DEGREE PROJECT IN TECHNOLOGY,
FIRST CYCLE, 15 CREDITS
STOCKHOLM, *SWEDEN 2019*

Direct detection of dark matter

MATHIAS AXELSSON

NIKLAS NYHOLM

KTH ROYAL INSTITUTE OF TECHNOLOGY
SCHOOL OF ENGINEERING SCIENCES

EXAMENSARBETE INOM TEKNIK,
GRUNDNIVÅ, 15 HP

STOCKHOLM, *SVERIGE 2019*

Direkt detektion av mörk materia

MATHIAS AXELSSON

NIKLAS NYHOLM

KTH
SKOLAN FÖR TEKNIKVETENSKAP

Abstract

Despite accounting for almost 85 % of all mass in the Universe, the properties of dark matter are mostly unknown. While some of this unknown matter can be explained by the standard model, the properties of the rest are unspecified. The most common explanation is an unknown particle that can interact with baryonic matter. If that is true, dark matter could be detected through weak interactions with other particles. In this report we will explain some evidence for dark matter and discuss different avenues of detecting dark matter while focusing on direct detection. We will examine theoretical detection rates and their dependencies. Finally we will examine numerically calculated expected total number of detector events, compare them to experimental total number of detector events and discuss current efforts in direct detection of dark matter.

Sammanfattning

Trots att nästan 85 % av all massa i universum består av mörk materia är dess egenskaper okända. Medan vissa delar av den okända materian kan beskrivas med hjälp av standardmodellen, är egenskaperna av den övriga oidentifierad. Den vanligaste förklaringen är en okänd partikel som kan interagera med baryonisk materia. Om partikeln finns kommer den att kunna bli detekterad genom svag växelverkan med andra partiklar. I denna rapport presenteras bevis för existensen av mörk materia. Dessutom kommer olika metoder att detektera den okända materian diskuteras, där största fokuset ligger på direkt detektion. I rapporten kommer det teoretiska antalet detektionsutfall och dess beroenden att undersökas. Slutligen kommer det förväntade totala antalet beräknade detektionsutfall att studeras. Dessa resultat kommer att jämföras med totala antalet utfall hos existerande experiment.

Acknowledgements

We would like to thank our supervisor Mattias Blennow, for answering our questions and pushing us in the right direction during the project. In addition we would like to thank everyone that helped us proofread our work.

Contents

Chapter 1

Introduction

Nearly 85 % of all matter in the Universe consists of dark matter [1]. Despite being the most common type of matter, it is the matter scientists know the least about. Neither the mass nor the strength of its interactions are known. Different theories have been proposed and most of them explain the missing mass with unknown particles [2]. The detection of these particles has been the subject of a number of different experiments that systematically limit the properties of dark matter.

This report will present a short section containing background information, including evidence for the existence of dark matter, such as rotational velocities of galaxies, and discrepancies between different types of measurements of the mass of galaxies. Then different methods for detecting dark matter will be presented. This report will focus on direct detection of dark matter. Theoretical formulas will be used to calculate expected detector rates for a general detector. Finally the model presented will be compared with the results from a real direct detection experiment.

Chapter 2

Background Material

2.1 Evidence for dark matter

There are several indications of the existence of dark matter in the Universe. In this section we will go through three different methods for inferring the existence of dark matter. First we will examine velocity curves in galaxies and infer the existence of extra mass that cannot be seen by telescopes. Afterwards other evidence for dark matter will be presented.

2.1.1 Rotational velocities in galaxies

By using Newton's law of universal gravitation and the formula for the centripetal force the orbital velocity of an object orbiting a galaxy with radius greater than the galactic disk $r > R_{\text{disk}}$ should roughly follow

$$v(r) = \sqrt{\frac{GM}{r}}, \tag{2.1}$$

where we have assumed that the distribution is spherically symmetric. G is the gravitational constant, M is the mass of the galaxy, and r is the distance from the galaxy's centre. However, when studying the velocities on the edges of galaxies it seems like the orbital velocities stay roughly constant with increasing distance from the centre of the galaxy [3]. This in turn implies that $M(r) \propto r$ and that part of the mass of the galaxy extends beyond the visible disc [1]. This anomaly is an indication of dark matter. In figure 2.1 two examples of rotational curves are shown based on data sets from SPARC [4]. The blue line shows the orbital velocities from observed data and the red line shows the contribution of expected velocities from baryonic matter. From these rotational curves and the rotational curves from Rubin *et al.* [3] it is possible to infer that the density distribution of the dark matter is approximately

$$\rho(r) \propto \frac{M(r)}{r^3} \propto \frac{1}{r^2}. \tag{2.2}$$

We have assumed that the unknown matter is symmetrically distributed in a spherical halo around the center of the galaxy. However, this assumption is a simplification and therefore the real distribution will differ from equation (2.2).

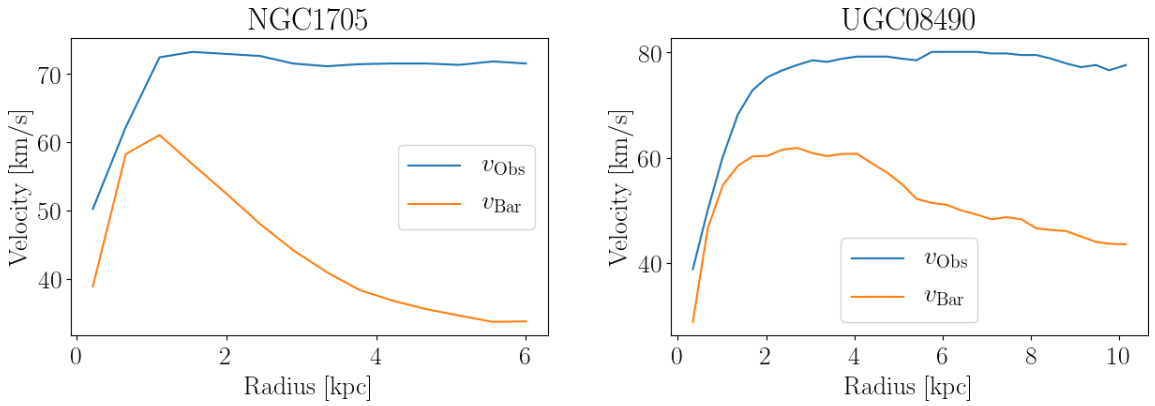

Figure 2.1: Rotation curves for NGC1705 (left) and UGC08490 (right). The blue lines show the observed data and the orange lines show the velocity expected from from baryonic matter. Data from SPARC [4].

2.1.2 Gravitational lensing

One of the results of Einstein's theory of general relativity is that gravity bends the direction light travels [5], which has given us another hint of the existence of dark matter. A result of this is that galaxies bend the light of other galaxies behind them relative to us. This is called gravitational lensing. By looking at objects through the gravitational lens it is possible to measure the mass of galaxies as well as learn about the distribution of dark matter and thus the mass of the dark matter halo [2].

2.1.3 ΛCDM model

ΛCDM model (Λ Cold Dark Matter) indicates that dark matter particles that never traveled at relativistic velocities (cold dark matter) [2] are an important part of the Universe. Measurements of the temperature anisotropies in the cosmic microwave background made by WMAP [6] and the Planck satellite [7] has given us data which, when compared with the ΛCDM model confirms the models predictions with high significance. Current estimates show that approximately 26.5 % of the energy density in the Universe consists of dark matter. Furthermore supercomputers using this model have executed N-body simulations with matter and dark matter particles to describe the expansion history of the Universe. These simulations show similar results to observed data from galaxy surveys [8, 9, 10].

2.2 What is dark matter?

The evidence for the existence of some sort of dark matter is clear. However, the evidence gives very few clues to what the extra mass consists of. While this report will focus on the direct detection of a dark matter particle we have included other theories that do not rely on a dark matter particle.

2.2.1 MACHOs

Massive Astrophysical Compact Halo Objects or MACHOs are macroscopic objects that emit low amounts of radiation and are therefore only detectable through their gravitational interactions. MACHOs are believed to be at most a part of the explanation for dark matter. Examples of these objects are black holes, neutron stars, brown dwarfs, and planets without any planetary system [2]. However, MACHOs can not fully explain dark matter. Observations of gravitational microlensing have shown that between 8 % and 50 % of the dark matter halo consists of MACHOs at 95 % confidence level [11]. The observations also find that a halo consisting of 100 % MACHOs is ruled out at the same confidence level. MACHOs are thus most likely a part of a dark matter halo, but can not account for the whole mass of the halo.

2.2.2 MOND

While this report aims to explore dark matter detection, Modified Newtonian dynamics or MOND [12] proposes that instead of dark matter, Newton's laws should be modified for small accelerations. Milgrom's proposal for a modification to Newton's second law of motion is

$$m\mu\left(\frac{a}{a_0}\right)\mathbf{a} = \mathbf{F}, \tag{2.3}$$

where μ is a function defined by

$$\mu(x) \approx \begin{cases} 1 & \text{if } x \gg 1 \\ x & \text{if } x \ll 1 \end{cases}. \tag{2.4}$$

However, MOND only predicts galaxy rotational curves and results from gravitational lensing. It does not predict larger scale structures in a satisfactory manner [2]. These as well as other problems make MOND an unsatisfactory answer to what the missing mass is.

2.2.3 Standard model candidates

In most of the literature, the dark matter particles are assumed to be massive and neutral with a weak self interaction [2]. The only known particle from the standard model that could be considered is the neutrino. The neutrino is a hot dark matter candidate due to its relativistic velocity in the early Universe. However, cosmological simulations of the structure of a neutrino dominated Universe do not agree with galaxy surveys [13], which make it unlikely that the neutrino is a valid dark matter candidate. Additionally, as a result of the fermionic character of the neutrino, the distribution of neutrinos is decided by the Fermi-Boltzmann distribution, which do not fit with the observed dark matter density in the halos [2].

2.2.4 Axions

In the standard model, quantum chromodynamics (QCD) which describes quarks and their interactions [14], generally allows CP-violation (charge conjugation parity violation). If the particle is interchanged with its antiparticle (charge conjugation) and the spatial

coordinates are inverted (parity), the CP-symmetry states that the law of physics should stay the same as in our Universe [15]. However, CP-violation has not been observed. The problem can be addressed by introducing a new theoretical particle, the axion. In addition to solving the CP-problem, the axion turned out to be a good dark matter candidate [2].

2.2.5 WIMPs

Weakly interacting massive particles, or WIMPs are another dark matter candidate. WIMPs are not a specific particle, but there are a number of characteristics that a WIMP candidate should possess. WIMPs do not exist in the standard model [2]. These particles should have no electric charge, a mass in the range from 1 GeV/c^2 to 100 TeV/c^2 and they should interact with normal matter through elastic scattering [16]. Extensions of the standard model such as the Minimal Supersymmetric Standard Model (MSSM) predict the neutralino [17]. It is a good WIMP candidate as it is stable and interacts weakly. However, it is only the lightest of the four neutralinos that is stable. For it to be stable, the so called R-parity needs to be conserved. R-parity relates the baryon numbers, lepton numbers, and spin of a particle. Standard model particles have $R = 1$ and their supersymmetric counterparts have $R = -1$. If R-parity is conserved, then the lightest supersymmetric particle will be stable which makes the lightest neutralino in the MSSM a good WIMP candidate.

Another viable WIMP candidate is the lightest Kaluza-Klein particle [18]. The idea is that there exist a number of extra dimensions in which the standard model fields can propagate. Similarly to the MSSM and the lightest supersymmetric particle, the lightest Kaluza-Klein particle is implied to be stable if Kaluza-Klein parity is preserved.

2.3 Detection of dark matter

There are three types of methods used in the search for the dark matter particle: indirect detection, products from particle collision, and direct detection [2]. In this section all the detection methods will be summarized. Figure 2.2 shows the possible detection channels.

2.3.1 Indirect detection

Indirect detection experiments search for the products of dark matter annihilation [1]. A pair of dark matter particles can annihilate into a pair of standard model particles, which can decay further to γ-rays, neutrinos, $p\bar{p}$, or e^+e^- [2]. The particles then propagate through space and can be detected by a telescope on Earth or by a satellite.

2.3.2 Particle collision

By colliding standard model particles and searching for events with missing energy or transverse momentum, it is possible to infer the existence of dark matter candidate [2]. This experiment can be a complement to direct detection and indirect detection. If a new suitable dark matter candidate is detected by direct detection or indirect detection, collision experiments can try to produce the new particle and study its properties. The same holds the other way around; if a new dark matter candidate is produced in a particle

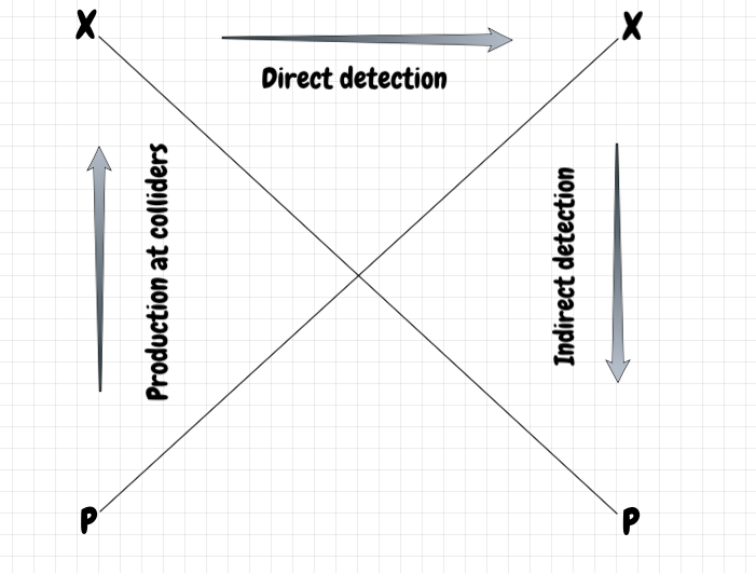

Figure 2.2: Schematic representation showing the possible detection channels, P is a standard model particle and χ is a dark matter particle. In the upward direction collision of standard model particles can produce pair of dark matter particles. In the downward direction two dark matter particles can annihilate to pairs of standard model particles. The direction from left to right shows that dark matter particles can interact weakly with standard model particles.

collision experiment, then the indirect detection and direct detection experiments can search for this new particle [19].

2.3.3 Direct detection

Direct detection aims to detect recoils from interactions of dark matter particles with target nuclei in detectors [1]. Assuming the dark matter particle has a mass in range from 10 GeV/c^2 to 1 TeV/c^2, the interaction would produce a recoil energy in the range from 1 keV to 100 keV. The recoil energy from the interaction is very small and therefore it is important for the detector to be very sensitive.

Signatures of dark matter in direct detection

Measurements of the energy dependence of dark matter interactions is the most common approach in direct detection experiments [2]. Due to the Earth's rotation around the Sun, there is an annual time dependence of the speed of dark matter particles relative to the Earth. The speed will be largest in June and smallest in December. Therefore some of the scattering events will have a larger recoil energy in June than in December, consequently the differential rate dR/dE_R will have a so called annual modulation. This annual modulation of the differential rate improves the capability of discriminating dark matter signals from background signals.

There is another dark matter signature called directionality [2]. The interaction between a nucleus and a dark matter particle will create a nuclear recoil with a certain direction, which has a strong angular dependence. Therefore the number of scattering

events above the detector's threshold energy will be an order of magnitude greater in one direction in comparison to the oposite direction. In the same way as annual modulation, directionality enhances the ability to discriminate possible a dark matter signal from backgrounds.

Background sources

One of the biggest challenges in the direct detection experiment is to reduce the background [2]. Some of the background comes from γ-rays due to decay of natural isotopes of uranium, thorium, potassium, cobalt, and cesium in the neighboring material. γ-rays can interact with matter by Compton scattering, photoelectric effect, or e^-e^+ pair production. These types of interactions result in the emission of an electron with a certain energy. If the energy matches the energy region of interest in the dark matter search, the sensitivity of the experiment can be affected. The experimental setup can be shielded from surrounding γ-rays with materials with a high density. This means the material has a good power of absorption. To fulfill this purpose, lead is a common choice. The detector can also be protected by a large tank of water, which gives a homogeneous shielding.

There are other background sources, such as neutrons, that can interact with the detector nuclei producing nuclear recoils. Cosmogenic neutron radiation occurs due to interactions of muons with nuclei in the detector material or the surrounding material [2]. The detector is normally placed deep underground to minimize the cosmogenic neutron radiation as the muon flux gets lower the deeper underground the detector is placed. This is important because the neutron-nucleus scattering signal is identical to the one of the dark matter particles. Neutron radiation also appears when traces of uranium disintegrates by spontaneous fission, this is called radiogenic neutron radiation [2]. Material with low uranium and thorium content gives lower neutron radiation from spontaneous fission, which reduces these kind of backgrounds [2].

As the threshold energies of the detector decrease and the detector target mass increases, the experiment becomes sensitive to neutrino signals. Coherent solar neutrinos that originate from nuclear fusion powering the Sun [20] will be a significant background to dark matter experiments for smaller dark matter masses around a few GeV/c^2 with a cross section of approximately 10^{-45} cm^2 [2]. Additionally, at large dark matter particle masses with cross sections around 10^{-49} cm^2, will be sensitive to the coherent scattering of atmospheric neutrinos, which result from interactions of atomic nuclei from the Earth's atmosphere with cosmic radiation [2, 20]. Neutrinos and dark matter particles have an annual modulation, which can be used to distinguish the two particles from each other. The detection rate of dark matter particles have a peak around June, while the detection rate of solar neutrinos and atmospheric neutrinos have a peak around January [2].

These external background sources are common to all types of detectors. However, different types of detectors will have additional internal backgrounds that decreases their sensitivity [2].

Detector technology

There exists many different technologies for direct detection of dark matter. The detector has to be sensitive to small recoil energies, moreover it must distinguish background events from dark matter events. To increase the probability of interactions in the detector, the target mass must be large. Additionally, it is important that the detector can be active

over long periods of time [2]. The signal consists of the production of heat, ionization, or emitted photons.

Particle physics scintillators is one of the more common detector types. A scintillating material is excited by radiation passing through it. The de-excitation causes the emission of light [2]. In searches for dark matter, sodium-iodine (NaI) or cesium-iodine (CsI) crystals are used. Impurities of thallium are put into the crystals to shift the emitted light to more favorable wavelengths for detection. Scintillators have an advantage because they are simple to use compared to other technologies. This allows scintillators to operate for long periods of time. A disadvantage is that the technology can not distinguish standard model particles and dark matter from each other.

Germanium detectors can be used to search for dark matter with a mass of a few GeV/c^2. Dark matter is detected via ionization, which makes the detector unable to separate dark matter signatures from background signatures [2]. Germanium detectors have a very low energy threshold, which leads to sensitivity to dark matter with low mass. During operation the detector is cooled to 77 K, which is easy to achieve relative to other detectors' requirements.

Another group of detectors is the liquid noble gas detectors. These are a subset of scintillators using liquid noble gasses such as argon or xenon [2]. The targets can be large and homogeneous which is one of the main advantages. Another advantage for xenon-based detectors is that they contain a little less than 50 % of isotopes with a nonzero spin. This makes this type of detector sensitive to spin-dependent interactions. The target mass is usually contained in a sphere which with the help of the timings of the sensors, can pinpoint the position of the collision with cm resolution.

Spin dependence for dark matter

Dark matter-nucleon interactions can have a spin-dependent contribution and a spin-independent contribution. To detect spin-dependent interactions, an isotope with a nuclear ground state angular momentum $J_N \neq 0$ is needed according to Abdelhameed *et al.* [21]. Abdelhameed *et al.* proposes lithium as a detector material as its most abundant isotope has a nuclear ground state angular momentum $J_N = 3/2$ and a spin of $1/2$. In addition lithium is a light element and is therefore suited to search for light spin-dependent dark matter. However, in this report we will assume that the interactions are spin-independent.

Chapter 3

Investigation

3.1 Problem

The aim of this investigation is to numerically calculate the expected total number of events for a given a dark matter mass m_χ and a dark matter-nucleon cross section σ_p. Furthermore, we will statistically analyze our theoretical results. Finally we will relate this to current literature and expectations for dark matter direct detection.

3.2 Model

3.2.1 Differential rate

The expected differential rate dR/dE_R [1/(s kg KeV)] following from Lisanti [1] is written in the form

$$\frac{dR}{dE_R} = \frac{\rho_\chi}{m_\chi m_T} \int_{v_{\min}}^{v_{\max}} v f(\mathbf{v}, t) \frac{d\sigma(E, \mathbf{v})}{dE_R} dv^3, \tag{3.1}$$

where $f(v, t)$ is the velocity distribution in the lab frame, which has a time dependence due to the Earth's movement relative to the Sun. The variable ρ_χ is the local dark matter density. We will use the dark matter density 0.3 Gev/c^2, which comes from results of mass modeling the Milky Way and is in good agreement with data from galactic surveys [22]. The variables m_χ and m_T are the masses of the dark matter particle and the nucleus target, respectively. The variable $v_{\min}$ is the minimum velocity required to produce nuclear recoils with energy E_R and $v_{\max}$ is the escape velocity of our galaxy. We will use $v_{\max} = 544$ km/s, which is the calculated likelihood median using data from the RAVE survey [23]. The variable $d\sigma/dE_R$ is the differential scattering cross section, which will be discussed later.

We can derive an expression for $v_{\min}$ [24] as follows: The recoil energy from the collision with resulting momentum transfer $\mathbf{q}$, and target nucleus with mass m_T is

$$E_R = \frac{\mathbf{q}^2}{2m_T}. \tag{3.2}$$

If we let $\mathbf{p}_{\chi,1}$ be the momentum of the dark matter particle before collision and, $\mathbf{p}_{\chi,2}$ the momentum after collision, the momentum transfer is given by

$$\mathbf{q} = \mathbf{p}_{\chi,2} - \mathbf{p}_{\chi,1}. \tag{3.3}$$

The momentum of the system is 0 in the center of mass frame

$$\mathbf{p}_\chi + \mathbf{p}_T = 0, \tag{3.4}$$

where $\mathbf{p}_T$ is the momentum of the target nucleus and $\mathbf{p}_\chi$ is the momentum of the dark matter particle. The initial dark matter momentum in the center of mass frame is

$$\mathbf{p}_{\chi,1} = -\mathbf{p}_{T,1} = \mu_T \mathbf{v}, \tag{3.5}$$

where $\mu_T = m_\chi m_T/(m_\chi + m_T)$ is the reduced mass of the system of the dark matter particle and the target nucleus and $\mathbf{v}$ is the velocity of the system's centre of mass. Equations (3.3) and (3.5) give

$$\mathbf{p}_{\chi,2} = \mathbf{q} + \mu_T \mathbf{v}. \tag{3.6}$$

We are assuming that the collision is elastic, therefore according to momentum conservation we have that

$$|\mathbf{p}_{\chi,1}|^2 = |\mathbf{p}_{\chi,2}|^2, \tag{3.7}$$

where $\mathbf{p}_{\chi,1}$ and $\mathbf{p}_{\chi,2}$ are the momenta of the dark matter particle before and after collision, respectively. Equation (3.3) together with Eqs (3.6) and (3.7) gives

$$\mathbf{q}^2 = (\mathbf{p}_{\chi,2} - \mathbf{p}_{\chi,1})^2 = 2(\mathbf{p}_{\chi,1}^2 - \mathbf{p}_{\chi,2}\mathbf{p}_{\chi,1}\cos(\theta)) = 2(\mu v)^2[1 - \cos(\theta)]. \tag{3.8}$$

Equations (3.2) and (3.8) give an expression for the recoil energy

$$E_R = \frac{(\mu v)^2}{m_T}[1 - \cos(\theta))] \leq \frac{2(\mu v)^2}{m_T}, \tag{3.9}$$

which implies that

$$v_{\min} = \sqrt{\frac{m_T E_R}{2\mu}}. \tag{3.10}$$

3.2.2 Differential cross section

In this work we will examine spin-independent dark matter particle interactions. Therefore, only the spin-independent part of the differential cross section will be discussed. The spin-dependence is only relevant for nuclei with odd numbers of protons or neutrons [2]. The differential cross section $d\sigma/dE_R$ therefore becomes

$$\frac{d\sigma}{dE_R} = \frac{m_T}{2\mu_T^2 v^2}\sigma_{\text{SI}} F^2(q), \tag{3.11}$$

where m_T is the mass of the target nucleus, μ_T is the reduced mass for the target nucleus and the dark matter particle defined as $\mu_T = m_T m_\chi/(m_T + m_\chi)$, $F(q)$ is the form factor to be discussed later, and σ_{SI} is the spin-independent dark matter-nucleus cross section [1]. Different direct detection experiments use different target nuclei which would have different σ_{SI}. Therefore the dark matter-nucleon cross section σ_p is typically used instead. The cross section σ_{SI} and σ_p are related by

$$\sigma_{\text{SI}} = \frac{\mu_T^2}{\mu_p^2} A^2 \sigma_p, \tag{3.12}$$

where A is the mass number of the target nucleus and μ_p is the reduced mass of the nucleon-dark matter system, defined in the same fashion as μ_T.

3.2.3 The velocity distribution of dark matter

The rest frame for dark matter is generally assumed to be the galactic frame [1]. Dark matter particles in the halo of the Milky Way do not have a preferred direction of travel as they either do not interact with each other or do so very weakly. It is for this reason that dark matter does not collapse into a disc like baryonic matter. In this report we will use the velocity distribution [1],

$$f(\mathbf{v}) = \begin{cases} \frac{1}{N_{\text{esc}}} \left(\frac{3}{2\pi\sigma_v^2}\right)^{3/2} e^{-3\mathbf{v}^2/2\sigma_v^2} & : |\mathbf{v}| < v_{\text{esc}} \\ 0 & : \text{otherwise} \end{cases} \tag{3.13}$$

with $v_0 = \sqrt{2/3}\sigma_v \approx 235$ km/s and $N_{\text{esc}} = \text{erf}(z) - 2\pi^{-1/2} z e^{-z^2}$ with $z = v_{\text{esc}}/v_0$ as our dark matter velocity distribution. Here v_{esc} is the escape velocity from the Milky Way galaxy at the position of the Sun.

As it is the velocity distribution of dark matter in our galaxy's rest frame, this distribution does not take into account the motion of the Sun around the centre of the Milky Way or the motion of the Earth around the Sun [1]. To take these motions into account, we add them to the velocity $\mathbf{v}$. The velocity of the Sun around the Milky Way is approximately 220 km/s and the orbital velocity around the Earth is approximately 30 km/s. The latter motion also changes direction over the year, which needs to be taken into account. To apply these modifications we substitute $\mathbf{v}$ in Eq (3.1) with $\tilde{\mathbf{v}} = \mathbf{v} + \mathbf{v}_\oplus + \mathbf{v}_\odot(t)$, where $\tilde{\mathbf{v}}$ is the dark matter velocity in the Earth's reference frame, $\mathbf{v}_\oplus$ is the velocity of the Sun relative to the center of mass of Milky way, and $\mathbf{v}_\odot(t)$ is the orbital velocity of Earth around the Sun. The full integration over the velocity, including the velocity dependence of the differential scattering cross section, then becomes

$$\int_{v_{\text{min}}}^{v_{\text{esc}}} \frac{1}{|\mathbf{v}|} f(\tilde{\mathbf{v}}) d^3\mathbf{v}. \tag{3.14}$$

The time dependence can be simplified by noticing that $\mathbf{v}_\oplus \gg \mathbf{v}_\odot$. With this we can assume that the velocity vector of the Earth is always pointed in the same direction as the velocity vector of the Sun. This turns $\tilde{\mathbf{v}}$ into $\mathbf{v} + \mathbf{v}_\oplus\big[1 + v_\odot/v_\oplus \cos(\omega[t - t_0])\big]$.

3.2.4 Form factor

The form factor $F(q)$ is the final part of the formula to calculate the differential recoil spectrum. It relates the effective cross section of the target nucleus to the transfer of recoil momentum [25]. When the momentum transfer q gets larger the effective cross section decreases. The form factor used in this work is called the Helm form factor [26]

$$F(q) = 3e^{-(qs)^2/2} \, \frac{\sin(qr_n) - qr_n \, \cos(qr_n)}{(qr_n)^3}. \tag{3.15}$$

The two constants s and r_n are the nuclear skin thickness and the effective nuclear radius, respectively. The effective nuclear radius is defined by $r_n^2 = c^2 + \frac{7}{3}\pi^2 a^2 - 5s^2$, with $c \approx 1.23A^{1/3} - 0.6$ fm, $a \approx 0.52$ fm, and $s \approx 0.9$ fm. Here A is the isotope number of the target nucleus. These constants have all been derived experimentally. Similarly q is calculated from the recoil energy and the target nucleus mass

$$q = \sqrt{2m_T E_R}. \tag{3.16}$$

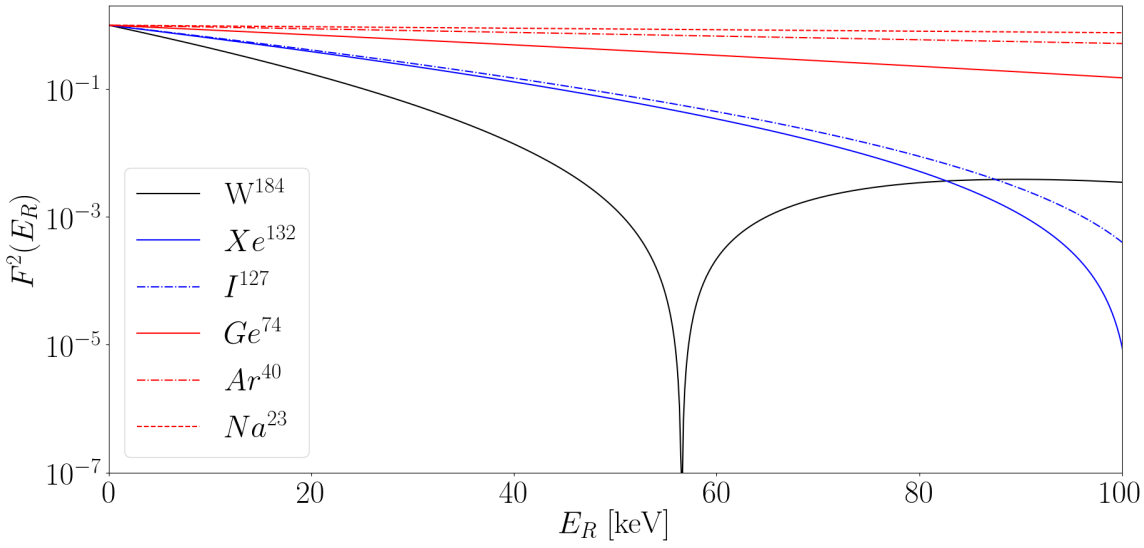

Figure 3.1: Comparison of form factors for different common target nuclei.

For this to hold, m_T, s, and r_n need to be expressed in natural units. If they are not, dimensional analysis shows that the exponent, sine, and cosine inputs need to be divided by $\hbar$. Figure 3.1 shows a comparison of $F^2(q)$ for different common target nuclei. Note that the heavier elements have a greater change in the form factor compared to lighter elements.

3.2.5 Particle data

As an approximation we have only used the atomic mass number of one isotope when calculating σ_{SI} in the differential cross section and c in the form factor. These isotopes are the most common one of each element according to Juris Meija *et al.* [27]. The atomic mass of each element used have been calculated by Juris Meija *et al.* [28].

3.3 Numerical Analysis

In this section we derive an expression for the expected differential rate, the expected rate, and the dark matter-nucleon cross section σ_p as a function of the dark matter mass. Finally we will discuss a method to test the statistical significance of an experimental result.

3.3.1 Differential rate

Equation (3.1) gives us the expected differential rate

$$\frac{dR}{dE_R} = \frac{\rho_x}{m_x m_T} \int_{v_{\min}}^{v_{\text{esc}}} v f(\mathbf{v} + \mathbf{v_{obs}}, t) \frac{d\sigma(E, v)}{dE_R} dv^3, \tag{3.17}$$

where $v_{\min}$ follows from Eq (3.10) and the differential cross section $d\sigma(E, v)/dE_R$ comes from Eq (3.11). The dark matter velocity distribution relative to the lab frame follows

from Eq (3.13),

$$f(\mathbf{v}+\mathbf{v_{obs}},t)=\begin{cases}\frac{1}{N_{\text{esc}}}\left(\frac{3}{2\pi\sigma_v^2}\right)^{3/2}e^{-3(\mathbf{v}+\mathbf{v_{obs}})^2/2\sigma_v^2} & :|\mathbf{v}+\mathbf{v_{obs}}|<v_{\text{esc}}\\ 0 & :\text{otherwise}\end{cases} \tag{3.18}$$

where $\mathbf{v}_{\text{obs}}=\mathbf{v}_{\oplus}\big[1+v_{\odot}/v_{\oplus}\cos(\omega[t-t_0])\big]$. The integral is numerically calculated in spherical coordinates, hence the integral takes the form

$$\frac{dR}{dE_R}=2\pi\frac{\rho_x}{m_x m_T}\int_0^{\pi}\int_{v_{\min}}^{v_{\max}}f(\mathbf{v}+\mathbf{v_{obs}},t)\frac{d\sigma(E,v)}{dE_R}v\sin(\theta)dvd\theta. \tag{3.19}$$

3.3.2 Total expected number of events

The total expected rate is determined by integrating over all expected recoil energies E_R in Eq (3.19),

$$R=\int_{E_{\min}}^{E_{\max}}\frac{dR}{dE_R}dE_R, \tag{3.20}$$

where $E_{\min}$ is the minimum energy the detector can detect and $E_{\max}$ is the maximum energy. To find the expected number of events we integrate R over the lifetime of the experiment and multiply the result with the detector mass. We denote the total number of expected events as N.

3.3.3 Cross section as a function of dark matter particle mass

To compare different types of detectors we can look at the cross section σ_p as a function of the dark matter particle mass m_χ. The expected total number of events is the simplest method of analyzing the data from a detector. We consider the combinations of mass m_χ and cross section σ_p that give rise to a given expected total number of events. These can then be plotted and used to compare different detector materials. To find this function we calculate an expected total number of events N_{fix} for a specified $\sigma_{p,\text{fix}}$ and $m_{\chi,\text{fix}}$. Afterward we take note that $N\propto\sigma_p$. For dark matter masses in range from 10 GeV/c^2 to 10 TeV/c^2 we calculate $N(\sigma_{p,\text{fix}},m_\chi)$. However,

$$N(\sigma_p,m_\chi)=\frac{N(\sigma_{\text{fix}},m_\chi)\sigma_p}{\sigma_{p,\text{fix}}}=N_{\text{fix}}, \tag{3.21}$$

and therefore,

$$\sigma_p(m_\chi)=\frac{N_{\text{fix}}\sigma_{p,\text{fix}}}{N(\sigma_{\text{fix}},m_\chi)}. \tag{3.22}$$

3.3.4 Rejection of expected total number of events

We will use statistical hypothesis testing to analyze if we can reject an extreme result with significance α. One event does not affect the probability for a second event to occur and therefore it is appropriate to use the Poisson distribution [29, p. 180]. We let our null hypothesis be that the expected total number of events N_{E} is correct and we want to test the null hypothesis with significance level α. The variable α is the probability of

rejecting the null hypothesis, given it was true. In addition, assume that the total number of events in an experiment $N_{\mathrm{M}} = 0$. The relationship between α, and N_{E} is

$$\frac{N_{\mathrm{E}}^0}{0!} e^{-N_{\mathrm{E}}} = \alpha, \tag{3.23}$$

and therefore,

$$N_{\mathrm{E}} = -\ln \alpha. \tag{3.24}$$

Given the significance level α and that the total number of events in an experiment is zero, we can reject the null hypothesis N_{E} with a significance level α [29, p. 320-324]. In this statistical analysis we have assumed that the experiment is ideal with no background.

3.4 Results

In this section we determine the expected total number of events for different detectors. Furthermore the differential rate is calculated and then plotted for different target masses in figure 3.2. Finally we plot the dark matter-nucleon cross section as function of the dark matter mass in figure 3.3.

3.4.1 Expected number of events

Table 3.1 shows the theoretical total number of events over one year for an experiment with target mass $m_T = 1000$ kg, given a dark matter-nucleon cross section $\sigma_p = 10^{-45}$ cm^2, and dark matter particle mass $m_\chi = 100$ GeV/c^2. This is done to illustrate the difference between different detector materials.

Target nucleus	^{184}W	^{132}Xe	^{127}I	^{74}Ge	^{40}Ar	^{23}Na
Detected events N	315	254	246	139	47	13

Table 3.1: Total number of events for a dark matter particle with $\sigma_p = 10^{-45}$ cm^2 and $m_\chi = 100$ GeV/c^2 from a detector with 1000 kg mass and 1 year of exposure. This idealized detector is able to detect recoil energies from 1 keV to 100 keV.

3.4.2 Differential rate spectrum

The differential rate spectrum shows dR/dE_R as a function of the recoil energy E_R. A comparison of the differential rates for different detector materials is shown in figure 3.2.

3.4.3 Bound on σ_p

To compare different types of detectors we look at the variations in the two relevant unknown properties of dark matter particles. By using the method described in section 3.3.3 we can compare detectors to each other.

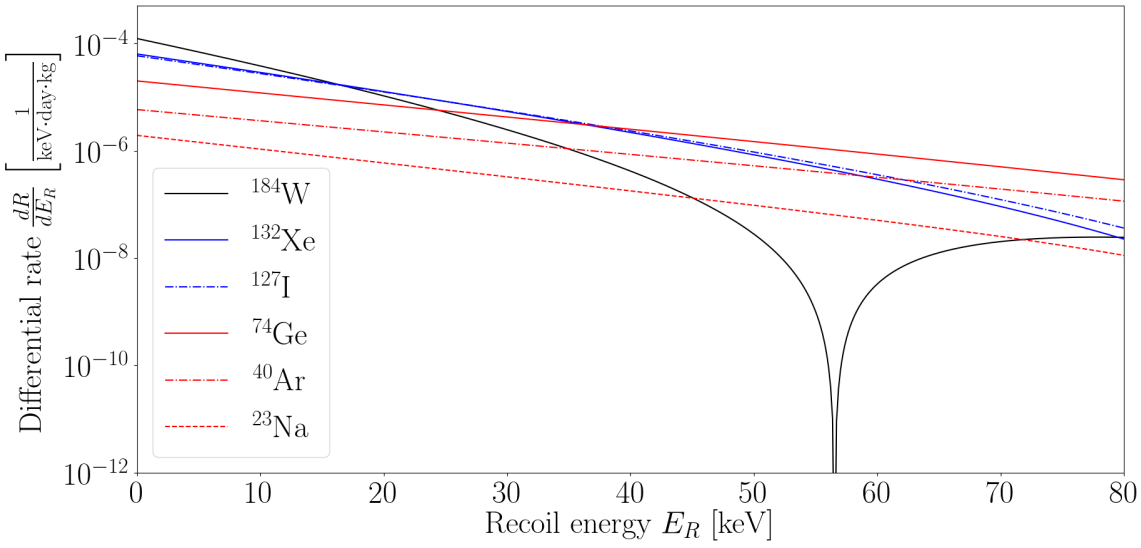

Figure 3.2: dR/dE_r as a function of the recoil energy E_R for dark matter particles with $\sigma_p = 10^{-45}$ cm^2 and $m_\chi = 100$ GeV/c^2.

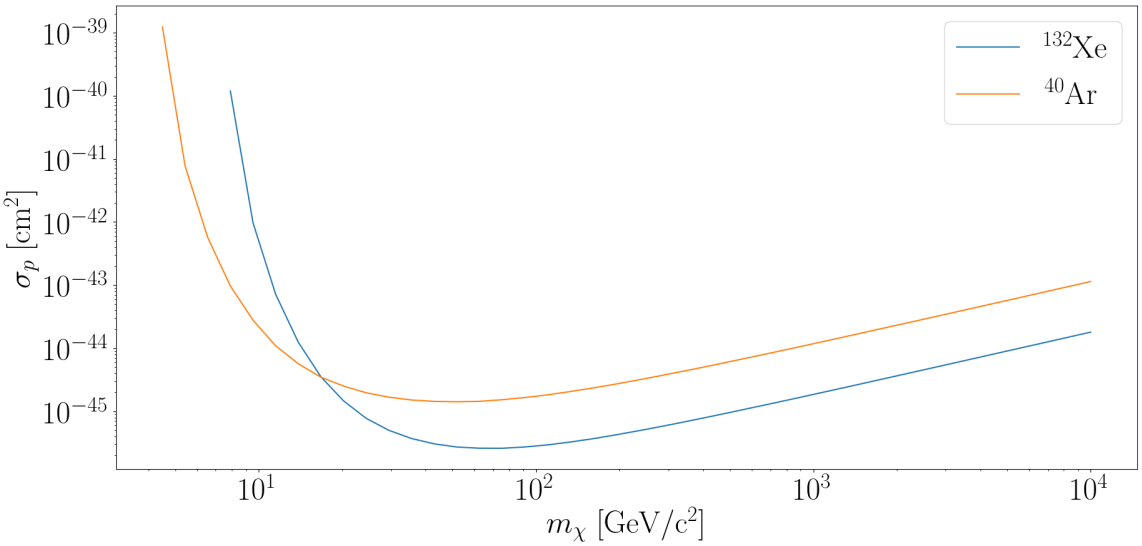

Figure 3.3: Variations in σ_p and m_χ for two different detector materials. The curves have been calculated with the same expected total number of events.

3.5 Discussion

3.5.1 Rejection of expected total number of events

Given that the hypothetical measured total number of events in a direct detection experiment is $N_\text{M} = 0$ and with the significance level $\alpha = 0.05$, the lower limit for the expected total number of events N_E that we can reject is

$$N_\text{E} = -\ln 0.05 \approx 3. \tag{3.25}$$

As a conclusion, the total expected number of events $N_{\mathrm{E}} = 3$ can be rejected with significance level $\alpha = 0.05$ if the total number of measured events in an experiment is zero. We can also reject any expected total number of events greater than 3 with significance level $\alpha = 0.05$ because the probability to measure a total number of events $N_{\mathrm{M}} = 0$ is smaller for larger N_{E}.

3.5.2 Differential rate spectrum

The differential rate spectrum dR/dE_R has a characteristic shape seen in figure 3.2. The differential rate is dependent on the form factor Eq (3.15), which implies that the differential rate $dR/dE_R = 0$ when $sin(qr_N) - qr_N cos(qr_N) = 0$. This can be seen in figure 3.2 for tungsten when $E_R \approx 57$ keV.

Additionally, figure 3.2 shows that the differential rate decreases with increasing recoil energy due to the exponential factor in the form factor. This gives us an insight into the importance of minimizing the detector's threshold energy in direct detection experiments.

3.5.3 Bound on σ_p

From figure 3.3 it is evident that lighter detector materials can detect lighter dark matter particles compared to heavier detector materials. This can be deduced by looking at which graph is lower in different intervals of the dark matter mass.

Both graphs in figure 3.3 have been calculated from the same expected total number of events. At lower masses the argon-40 graph has a smaller σ_p-value than the xenon-132 graph. In addition to a lower σ_p-value the argon-40 graph will also tend towards infinity at a lower m_χ-value. However, in section 3.4.1 we can also see that the expected total number of events decreases for lighter detector materials making those detectors more sensitive to noise. Longer exposure times have no effect on the lower bound of detectable dark matter particle masses as $R \propto \sigma_p$. This has the effect that an increased exposure time or a greater detector mass will only move the graph down and not left.

If we have rejected a expected total number of events using the method in section 3.3.4 the curves in figure 3.3 can be thought of as bounds for possible dark matter particle properties. As every point above the curve will have a higher expected total number of events those points can be rejected with a significance $< \alpha$, if the expected total number of events corresponding to the line have been rejected with a significance α. However, we can not conclude anything about points below the line.

3.5.4 Comparison with other literature

The calculated total number of events from section 3.4.1 comes from an idealized theoretical detector without background noise. A more realistic example can be taken from the Xenon1t experiment [30], which detects recoil energies between 4.9 keV and 40.9 keV. With this the Xenon collaboration expects to be sensitive to dark matter with masses from 6 GeV/c^2 and up. The most sensitive region is expected to be at $m_\chi = 30$ GeV/c^2 with $\sigma_p = 4.1 \cdot 10^{-47}$ cm^2. The experiment collected data for almost a year and the total exposure is 1 tonne yr. We can calculate $\sigma_p(m_\chi)$ from information in their paper and compare to their $\sigma_p(m_\chi)$-graph. From figure 3.5.4 we see that the Xenon1t experiment predicts a lower detectable dark matter particle mass than our calculations. This could

be because of the approximations described in section 3.2.5. In addition, our calculations predict a greater sensitivity to large dark matter masses. It is more likely however that this is caused by differences in our respective models. The ^{132}Xe graph has been calculated using detector properties from the Xenon1t experiment.

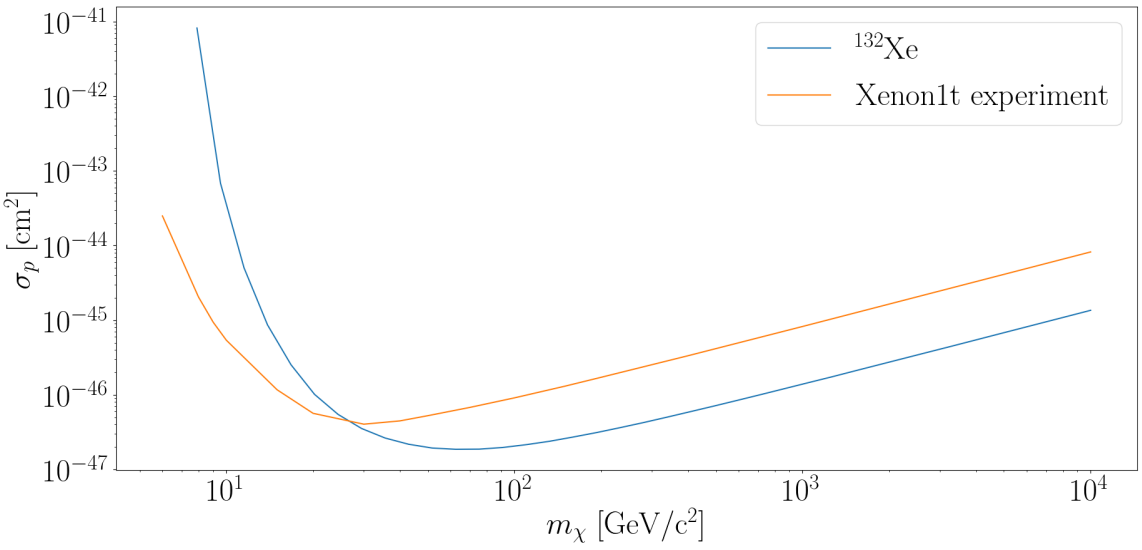

Figure 3.4: Comparison of confidence limits between the Xenon1t experiment and calculations from this report for spin independent dark matter particle-nucleus interactions. Data from the Xenon collaboration [30].

Chapter 4

Summary and Conclusions

We have in this report gone through some basic background information about dark matter and the methods used in the search for this unknown particle. In addition, we have numerically studied the differential detection rate for a given dark matter mass m_χ, dark matter nucleon cross section σ_p, and a given detector nucleus mass m_T. Moreover, as a result of the the differential rate we have calculated the expected total number of events. We could see that the differential rate is calculated by taking the averaged value for the differential scattering cross section $d\sigma(E, v)/dE_R$ over the incoming dark matter velocities. A crucial part of the differential scattering cross section is the form factor, which relates the recoil energy to the effective cross section. In this report we used the Helm form factor. It also is important that the velocity distribution is expressed in the lab frame, due to the Earth's rotational speed around the sun. Therefore $d\sigma(E, v)/dE_R$ has a time dependence.

Finally we plotted the dark matter-nucleon cross section as a function of the dark matter mass $\sigma_p(m_\chi)$. The function $\sigma_p(m_\chi)$ together with hypothesis testing gave us a method to reject an expected total number of events with a significance α given that the hypothetical measured total number of events in an experiment $N_{\mathrm{M}} = 0$.

Comparing our results to the Xenon1t experiment we found that there is a difference in the expected sensitivity for both lower and larger dark matter masses m_χ. The reason for this is not apparent but we suspect that this is either due to approximations made by us or differences in our calculations.

Bibliography

[1] Mariangela Lisanti. Lectures on Dark Matter Physics. Aug 2016, 1603.03797v2.

[2] Teresa Marrodán Undagoitia and Ludwig Rauch. Dark matter direct-detection experiments. *J. Phys.*, G43(1):013001, Mar 2017, 1509.08767v2.

[3] V. C. Rubin, W. K. Ford Jr., and N. Thonnard. Rotational properties of 21 SC galaxies with a large range of luminosities and radii, from NGC 4605 /R = 4kpc/ to UGC 2885 /R = 122 kpc/. *Astrophysical Journal*, 238:471–487, Jun 1980.

[4] F. Lelli, S. S. McGaugh, and J. M. Schombert. SPARC: Mass Models for 175 Disk Galaxies with Spitzer Photometry and Accurate Rotation Curves. *The Astronomical Journal*, 152:157, December 2016, 1606.09251.

[5] Ramesh Narayan and Matthias Bartelmann. Lectures on Gravitational Lensing. Feb 2008, arXiv:astro-ph/9606001v2.

[6] G. Hinshaw, D. Larson, E. Komatsu, D. N. Spergel, et al. Nine-Year Wilkinson Microwave Anisotropy Probe(WMAP) Observations: Cosmological Parameter Results. *The Astrophysical Journal Supplement Series*, 208(2):19, sep 2013.

[7] P. A. R. Ade et al. Planck 2013 results. I. Overview of products and scientific results. *Astron. Astrophys.*, 571:A1, 2014, 1303.5062.

[8] Volker Springel, Simon D. M. White, Adrian Jenkins, Carlos S. Frenk, et al. Simulating the joint evolution of quasars, galaxies and their large-scale distribution. *Nature*, 435:629–636, 2005, astro-ph/0504097.

[9] Joop Schaye et al. The EAGLE project: Simulating the evolution and assembly of galaxies and their environments. *Mon. Not. Roy. Astron. Soc.*, 446:521–554, 2015, 1407.7040.

[10] Mark Vogelsberger, Shy Genel, Volker Springel, Paul Torrey, et al. Introducing the Illustris Project: Simulating the coevolution of dark and visible matter in the Universe. *Mon. Not. Roy. Astron. Soc.*, 444(2):1518–1547, 2014, 1405.2921.

[11] C. Alcock, R. A. Allsman, D. R. Alves, T. S. Axelrod, et al. The MACHO project: Microlensing results from 5.7 years of large magellanic cloud observations. *The Astrophysical Journal*, 542(1):281–307, Oct 2000, arXiv:astro-ph/0001272.

[12] M. Milgrom. A modification of the Newtonian dynamics as a possible alternative to the hidden mass hypothesis. *Astrophysical Journal*, 270:365–370, July 1983.

[13] Simon D. M. White, C. S. Frenk, and M. Davis. Clustering in a Neutrino Dominated Universe. *Astrophys. J.*, 274:L1–L5, 1983. [,80(1984)].

[14] Andrey Grozin. Quantum Chromodynamics. In *Proceedings, 11th International Baikal Summer School on Physics of Elementary Particles and Astrophysics: Bolshie Koty, Irkutsk region, Russia, July 3-10, 2011*, 2012, 1205.1815.

[15] Antonio Pich. Flavour Dynamics and Violations of the CP Symmetry. *CERN Yellow Rep. School Proc.*, 4:65, 2018, 1805.08597.

[16] P. Cushman, C. Galbiati, D. N. McKinsey, H. Robertson, T. M. P. Tait, et al. Snowmass CF1 Summary: WIMP Dark Matter Direct Detection. Nov 2013, 1310.8327v2.

[17] Gerard Jungman, Marc Kamionkowski, and Kim Griest. Supersymmetric dark matter. *Physics Reports*, 267(5):195 – 373, 1996.

[18] Géraldine Servant and Tim M.P. Tait. Is the lightest kaluza–klein particle a viable dark matter candidate? *Nuclear Physics B*, 650(1):391 – 419, 2003.

[19] Marta Felcini. Searches for Dark Matter Particles at the LHC. In *53rd Rencontres de Moriond on Cosmology La Thuile, Italy, March 17-24, 2018*, 2018, 1809.06341.

[20] J. W. F. Valle. Neutrino physics from A to Z : two lectures at Corfu. *PoS*, CORFU2016:007, 2017, 1705.00872.

[21] A.H. Abdelhameed, G. Angloher, P. Bauer, A. Bento, et al. First results on sub-GeV spin-dependent dark matter. 2019, 1902.07587.

[22] Anne M. Green. Astrophysical uncertainties on direct detection experiments. *Mod. Phys. Lett.*, A27:1230004, 2012, 1112.0524.

[23] Martin C. Smith et al. The RAVE Survey: Constraining the Local Galactic Escape Speed. *Mon. Not. Roy. Astron. Soc.*, 379:755–772, 2007, astro-ph/0611671.

[24] Tess W. P. Jacobson and Mariangela Lisanti. Velocity dependence of dark matter electron scattering. 2018.

[25] J.D. Lewin and P.F. Smith. Review of mathematics, numerical factors, and corrections for dark matter experiments based on elastic nuclear recoil. *Astroparticle Physics*, 6(1):87 – 112, 1996.

[26] Richard H. Helm. Inelastic and Elastic Scattering of 187-Mev Electrons from Selected Even-Even Nuclei. *Phys. Rev.*, 104:1466–1475, 1956.

[27] Juris Meija, Tyler B. Coplen, Michael Berglund, Willi A. Brand, et al. Isotopic compositions of the elements 2013 (iupac technical report). *Pure and Applied Chemistry*, 88(3):293–306, Feb 2016.

[28] Juris Meija, Tyler B. Coplen, Michael Berglund, Willi A. Brand, et al. Atomic weights of the elements 2013 (iupac technical report). *Pure and Applied Chemistry*, 88(3):265–291, Feb 2016.

[29] Gunnar Blom, Jan Enger, Gunnar Englund, Jan Grandell, and Lars Holst. *Sannolikhetsteori och statistikteori med tillämpningar*. Studentlitteratur AB, 5:14 edition, 2016. ISBN 978-91-44-02442-4.

[30] E. Aprile, J. Aalbers, F. Agostini, M. Alfonsi, et al. Dark matter search results from a one ton-year exposure of xenon1t. *Phys. Rev. Lett.*, 121:111302, Sep 2018.